**Articles in PresS. J Neurophysiol (July 20, 2016). doi:10.1152/jn.00991.2015**



# Distinct neural mechanisms for spatially lateralized and spatially global visual working memory representations.

Keisuke Fukuda[1], Min-Suk Kang[2,3], & Geoffrey F. Woodman[1]

[1]Department of Psychological Sciences, Vanderbilt University, Nashville, USA
[2]Center for Neuroscience Imaging Research, Institute for Basic Science, Suwon, Republic of Korea
[3]Department of Psychology, Sungkyunkwan University, Seoul, Republic of Korea

Correspondence to:
Keisuke Fukuda
PMB 407817
2301 Vanderbilt Place
Vanderbilt University, Nashville, TN 37240-7817
E-mail: keisuke.fukuda@vanderbilt.edu

Abstract

Visual working memory (VWM) allows humans to actively maintain a limited amount of information. Whereas previous electrophysiological studies have found that lateralized event-related potentials (ERPs) track the maintenance of information in VWM, recent imaging experiments have shown that spatially global representations can be read out using the activity across visual cortex. The goal of the present study was to determine whether both lateralized and spatially global electrophysiological signatures coexist. We first show that it is possible to simultaneously measure lateralized ERPs that track the number of items held in VWM from one visual hemfield and parieto-occipital alpha (8-12Hz) power over both hemispheres indexing spatially global VWM representations. Next, we replicated our findings and went on to show that this bilateral parieto-occipital alpha power as well as the contralaterally-biased ERP correlate of VWM carries a signal that can be used to decode the identity of the representations stored in VWM. Our findings not only unify observations across electrophysiology and imaging techniques, but also suggest that the ERPs and alpha-band oscillations index different neural mechanisms that map on to lateralized and spatially global representations, respectively.

Key Words: Visual working memory, Event-related potentials, EEG Oscillation

## New & Noteworthy

Our work shows that there exist lateralized and spatially global visual working memory (VWM) representations concurrently in mind, and that VWM representations are supported by dissociable electrophysiological correlates measured by human scalp EEGs. Our work not only bridges the gap between recent fMRI studies and more traditional electrophysiological event-related potential (ERP) studies of VWM, but also provides novel insight into the organization of VWM representations.

Visual working memory (VWM) allows us to store a limited amount of information, that we use to reason, solve problems, and have a coherent experience across interruptions in visual input (Fukuda et al., 2010, Unsworth et al., 2014a). Previous studies have shown that storing information in VWM results in lateralized electrophysiological activity. In contrast, functional magnetic resonance imaging (fMRI) studies have shown that non-lateralized VWM activity dominates during the retention interval of short-term memory tasks. That is, objects presented in one visual hemifield (e.g., left of fixation) elicit a sustained pattern of activity across multiple areas in visual cortex (Ester et al., 2009, Harrison and Tong, 2009, Serences et al., 2009, Pratte and Tong, 2014). Our goal here was to determine if we could find an electrophysiological counterpart of this spatially global signal coexisting with the already established lateralized event-related potentials (ERPs).

By recording subjects' ERPs, Vogel and colleagues (2004) demonstrated the existence of an electrophysiological correlate of VWM maintenance called the contralateral delay activity (CDA). In their experiments, subjects were first directed by a central arrow cue to remember objects presented in either the left or right hemifield. Next, a bilateral array of colored squares was presented. Subjects remembered as many colored squares as possible from the cued side. After a 1-second retention interval, subjects reported whether or not the colors in the test array matched those from the initial memory array. During the retention interval, parieto-occipital channels contralateral to the task-relevant hemifield showed a sustained negativity compared to ipsilateral channels. This CDA was further linked to VWM storage because it increased in amplitude up to individual subject's VWM capacity, plateauing across set sizes beyond one's capacity.

In contrast to these electrophysiological experiments that focused on lateralized activity, recent fMRI studies indicate that VWM may maintain spatially global representations (Ester et al., 2009, Harrison and Tong, 2009, Pratte and Tong, 2014). Ester and colleagues (2009) used multi-voxel patterns (MVPs) of BOLD responses to decode the content of visual cortex (i.e., areas V1-V4) during the retention interval of a VWM task. The representations in VWM were reliably decoded from the contralateral visual cortex. Surprisingly, Ester and colleagues (2009) also reliably decoded the contents of VWM from the ipsilateral MVPs. This indicates that ipsilateral brain areas participate in representing information in VWM, thus suggesting the existence of spatially global VWM representations in the brain.

Is it the case that electrophysiological and imaging techniques yield truly incompatible results regarding the nature of VWM representations? Or is it possible to simultaneously measure electrophysiological activity indexing spatially specific (i.e., lateralized) and spatially global representations in VWM? In Experiments 1 and 2, we tested the hypothesis that the CDA of the subjects' ERPs provides a metric of spatially specific VWM, while the simultaneously measured bilateral alpha activity of the EEG provides a metric of spatially global VWM. In addition, we show in Experiment 3 that both the lateralized ERPs and the spatially global oscillations can be used to decode the content of VWM, which verified their roles as neural correlates of VWM.

## Method and materials

Subjects

After obtaining informed written consent for procedures approved by the Vanderbilt University Institutional Review Board, we ran subjects with normal or corrected-to-normal vision in Experiment 1 (N=20), 2 (N=20) and 3 (N=24). They were compensated $10/hour for their participation. In Experiment 1 (12 men and 8 women) 3 additional subjects' data were excluded from analyses due to an excessive number of trials contaminated by ocular artifacts (more than 30% of trials in any condition). Similarly, in Experiment 2 (10 men and 10 women) 3 additional subjects' data were excluded, and in Experiment 3 (13 men and 11 women) 1 additional subject's data were excluded.

Procedure

Experiment 1

Subjects performed a bilateral change-detection task based on that used in Vogel and Machizawa (2004). Subjects were instructed to maintain fixation on a white central dot (0.2° in visual angle, x = 0.293, y = 0.323, 38.5 cd/$m^2$) presented on a gray background (x = 0.294, y = 0.322, 15.7 cd/$m^2$) throughout each trial of the experiment. After subjects initiated each trial with a button press, a central arrow cue was presented for 200ms. After the arrow cue offset, a cue-to-stimulus interval followed during which the screen was blank other than the fixation point. This Stimulus-Onset Asynchrony (SOA) was either 200ms (Short SOA) or 1000ms (Long SOA), randomly chosen with equal probability. We used these different SOAs to disentangle the activity related to selecting the task-relevant hemifield (i.e., shifts of spatial attention) from that related to actually maintaining information in VWM, as we will discuss in the Results section. The next event on each trial was the presentation of a bilateral stimulus array consisting of one, two, four, or eight colored squares in each hemifield for 150ms. Each set size was presented with equal probability and the different set sizes were randomly interleaved across trials. Each square subtended 0.7 x 0.7 degrees of visual angle, and the color was chosen from a set of 9 highly discriminable colors (red (x = 0.592, y = 0.367, 9.60 cd/$m^2$), green (x = 0.299, y = 0.579, 27.6 cd/$m^2$), blue (x = 0.15, y = 0.08, 4.35 cd/$m^2$), yellow (x = 0.396, y = 0.509, 35.5 cd/$m^2$), magenta (x = 0.295, y = 0.171, 13.3 cd/$m^2$), cyan (x = 0.219, y = 0.315, 31.2 cd/$m^2$), orange (x = 0.483, y = 0.447, 18.6 cd/$m^2$), black (x = 0.393, y = 0.423, 0.31 cd/$m^2$), and white (x = 0.293, y = 0.323, 38.5 cd/$m^2$) without repetition. The selected squares were distributed in a left and right rectangular area subtending 4.8 (horizontal) x 10.4 (vertical) degrees of visual angle whose center was 4.5 degrees away from the central fixation. After a retention interval of 850ms, during which the screen was blank other than the fixation point, a single test square was presented on the cued side. The subject indicated by a button press if the test square was the same color as the stimulus presented at the same location a moment ago. Subjects completed 200 trials at each set size and SOA combination.

Experiment 2

Subjects performed the same basic bilateral change-detection task used in Experiment 1 with the following modifications. First, the cue-to-stimulus SOA was fixed at 1000ms. Second, the set size in the task-relevant hemifield was one, four, or eight objects. These set sizes allowed us to more efficiently sample VWM loads both below

and above the subjects' capacity. Lastly, there were three different types of distractor conditions crossed with these three set sizes. In one condition, the number of distractors matched with the number of targets (termed the *matched distractor condition* because this is the typical procedure for measuring the CDA). In the next condition, there was only one distractor regardless of the number of targets (termed the *one-distractor condition*). In the last condition, there were always eight distractors regardless of the number of targets (termed the *eight-distractor condition*). We used these different distractor conditions to determine whether the electrophysiological measures were related to maintaining the different number of target items, or ignoring different numbers of distractors. Each distractor condition was presented in a separate block, with the order randomized across subjects. Each subject completed 200 trials in each combination of set size and distractor condition.

Experiment 3

Subjects in Experiment 3 performed a different VWM recall task. Instead of color being the critical feature with the set size varying across trials, subjects had to remember the orientation of one bar presented in the left or right visual field. This change of task allowed us to test the hypothesis that the scalp distribution of bilateral alpha-band activity as well as that of the CDA could be used to decode the orientation of the bar that subjects were holding in VWM.

After subjects initiated each trial with a button press, a central arrow cue was presented for 200ms to indicate the task-relevant hemifield for that trial (i.e., left or right). Then, 900ms after the offset of the arrow cue, one white oriented bar surrounded by a ring (ring radius = 1.6°, bar width = 0.5°) was presented in each hemifield (3.1° horizontal to the central fixation spot) for 200ms. For each trial, the orientation of the bar was randomly chosen from eight equally spaced seed angles (0°, 22.5°, 45°, 67.5°, 90°, 112.5°, 135°, 157.5°) and presented with a random jitter (range = ±11.25°). After a retention interval of 1000ms, one ring was presented on the cued side, and subjects reported the orientation of the bar by clicking where the bar met the ring using a computer mouse. Subjects completed 12 blocks of 128 trials.

EEG acquisition and pre-processing

The EEG was recorded using a right-mastoid reference, re-referenced offline to the average of the left and right mastoids. The signals were amplified with a gain of 20,000, a bandpass of 0.01-100 Hz, and digitized at 250 Hz. We used the 10-20 electrode sites (Fz, Cz, Pz, F3, F4, C3, C4, P3, P4, PO3, PO4, O1, O2, T3, T4, T5 and T6) and a pair of custom sites, OL (halfway between O1 and OL) and OR (halfway between O2 and OR). Eye movements were monitored using electrodes placed 1cm lateral to the external canthi for horizontal eye movements (i.e., the horizontal electrooculogram, or HEOG) and an electrode placed beneath the right eye for blinks and vertical eye movements (i.e., the vertical electrooculogram, or VEOG).

For each experiment, the continuous EEG data were first segmented into trial epochs. For Experiment 1, the trial epoch was defined as -400ms to 1200ms after the cue onset for Short SOA condition, and -400ms to 2200ms after the cue onset for Long SOA condition. For Experiment 2, the trial epoch was defined as -400ms to 2200ms after the cue onset. For Experiment 3, the trial epoch was defined as -400ms to 2200ms after the

cue onset. Trials accompanied by horizontal eye movements (> 30uV mean threshold across observers) or eye blinks (> 75uV mean threshold across observers) were rejected before further analyses. Subjects' data with more than 30% of trials rejected for ocular or motor artifacts in any given condition were excluded.

ERP analyses

To measure ERPs time-locked to the event of interest, we averaged the EEG responses across trials for each condition. The ERPs were baseline corrected using the potential measured from -400-0ms relative to the time-locking event. In other words, the mean amplitude in the baseline window was subtracted from the entire trial epoch. Based on the previous literature (Vogel and Machizawa, 2004, Fukuda and Vogel, 2009), we created grand-average contralateral and ipsilateral waveforms by averaging across parieto-occipital channels from P3/4, PO3/4, O1/2, OL/R, and T5/6 relative to the task-relevant hemifield. Then, we created a difference wave by subtracting the ipsilateral average from the contralateral average across the 5 pairs of posterior, lateralized channels. The mean amplitude from 300-1000ms after the memory array onset defined the CDA that we measured on each trial.

For Experiment 1, a two-way ANOVA with factors of set size (1, 2, 4, and 8) and SOA (short versus long) was run on the CDA data. For Experiment 2, separate one-way ANOVAs with a factor of set size (1, 4, and 8) were run for each distractor conditions. This was done because the matched distractor condition had varying number of distractors for each set size where as other conditions did not, thus making the distractor condition factor non-orthogonal to the other factor. To better examine the effect of distractors on the CDA, we ran an additional 2-way ANOVA (with the factors of set size and distractor condition) excluding matched distractor conditions.

EEG analyses

To examine the oscillatory responses, EEG from each trial was subjected to spectral decomposition with a fixed window size of 400ms and a window overlap of 380ms with a MATLAB function (spectrogram.m). Next, we measured the contralateral alpha power suppression using the following analysis steps. First, the baseline power spectrum was defined as the mean power spectrum observed in the pre-cue time window (-400 to 0ms relative to cue onset). This baseline spectrum was subtracted from the entire epoch and the resultant spectral difference was divided by the baseline spectrum and then multiplied by 100. This allowed us to calculate the percentage change in power at each frequency.

We created the contralateral and ipsilateral averaged alpha power (8-12Hz) by averaging the same set of the parieto-occipital channels as the CDA analysis (i.e., P3/4, PO3/4, O1/2, OL/R, and T5/6). Then we created a difference measure by subtracting the ipsilateral average from the contralateral average. This allowed us examine if there is a set-size dependent contralateral bias to the alpha power suppression.

To test the hypothesis that alpha power suppression is involved in representing information in VWM in a spatially global manner, we also examined contralateral and ipsilateral alpha power separately. Because we were interested in the oscillatory responses to the onset of the stimulus, we used the pre-stimulus time window (-400 to 0ms relative to stimulus onset) as the baseline to calculate alpha power responses for each

channel. Then, the same set of parieto-occipital channels were averaged to create contralateral and ipsilateral alpha power measures separately.

To test the bilateral alpha power suppression for Experiment 1, a three-way ANOVA with factors of set size (1, 2, 4, and 8), SOA (short versus long), and laterality (contralateral versus ipsilateral) was run. For Experiment 2, separate two-way ANOVAs with a factor of set size (1, 4, and 8) and laterality (contralateral versus ipsilateral) were run for each distractor condition. This was done because the matched distractor condition had varying number of distractors for each set size where as other conditions did not, thus making the distractor factor non-orthogonal to the set size factor. To better examine the effect of distractors on the bilateral alpha power suppression, we ran an additional 3-way ANOVA (with the factors set size, distractor, and laterality) excluding matched distractor conditions.

Decoding the contents of VWM

In Experiment 3, we determined if it was possible to reliably decode the content of VWM from the scalp distribution of both the lateralized ERPs and EEG oscillations. First, we divided the entire experimental session into 6 temporally defined epochs. Specifically, each epoch consisted of two consecutive experimental blocks with the first epoch being the first two blocks, the second epoch being blocks 3 and 4, and so forth. For the oscillatory signals, the power spectrum for each seed angle (0°, 22.5°, 45°, 67.5°, 90°, 112.5°, 135°, 157.5°) was averaged (average number of trials for each seed angle = 14) for each epoch. Using these averaged power spectra across channels as inputs, we trained separate linear classifiers (linear discriminant analysis, or LDA) for contralateral and ipsilateral channels. We did this for each frequency across each time-window from -200 to 1000 ms relative to stimulus onset[1] with a hold-one-out procedure. More precisely, the classifier was fed a set of power responses for a given frequency across contralateral (or ipsilateral) parieto-occipital channels (i.e., P3/4 PO3/4, O1/2, OL/R, and T5/6) observed in a given time window for each seed angle. Then, the classifier was trained using the data from 5 averaged epochs, before determining whether it could then classify the averaged data from the remaining epoch. This routine was repeated so that each epoch served as the test data. Once completed, we then moved on to a different frequency to cover the entire frequency range of interest (i.e., 2-30Hz). Then, we moved to a different time window and repeated the whole procedure. This analysis sequence provided a time course of classification accuracy for contralateral and ipsilateral power at each frequency, for each subject. As a control analysis, we also applied the same procedure to decode the content of the distractor orientation.

For the lateralized ERPs, we first calculated average amplitudes with the same sliding time windows as EEG data (i.e., a 400ms window with overlap of 380ms) for each parieto-occipital channel (i.e., P3/4, PO3/4, O1/2, OL/R, and T5/6). This was done to equate the temporal resolution of ERP-based and oscillation-based classifications for the purpose of direct comparison. We then created difference channels for each parieto-occipital channel pair by subtracting the amplitude of the ipsilateral channel from its contralateral counterpart. The resultant 5 difference channels were subjected to the same analytic sequence as the oscillatory signals.

[1] The time point indicates the center of the 400ms time window.

To address the potential alternative explanation that our decoding results were contaminated by small, but systematic eye movements, we applied the same decoding analysis to the EOG channels (i.e., the HEOG and VEOG channel). We first calculated average amplitudes for the same sliding time windows as EEG data (i.e., 400ms window with overlap of 380ms) for each EOG channel. Then, for each time window, we trained the classifier using the set of EOG channels from 5 epochs, and tested its accuracy on the remaining epoch. This procedure was repeated so that each epoch served as the test data.

Verifying the spatially global nature of posterior alpha power suppression

If the decoding ability of the scalp distribution of contralateral and ipsilateral alpha power in fact reflects the existence of spatially global VWM representations, then we should expect that contralateral and ipsilateral decoding performances are temporally synchronized. We tested by examining whether both contralateral and ipsilateral alpha power decoders output a correct response on the same trials. We compared against the assumption that contralateral and ipsilateral decoders predict the response based on independent evidence.

Regression analysis for decoding performance

To understand the relationship between lateralized and spatially global VWM representations, we examined the correlational structure among decoding accuracies based on different neural correlates of VWM. These correlates included the scalp distributions of contralateral and ipsilateral parieto-occipital alpha (8-12Hz) and theta (4-7Hz) power responses, and the scalp distribution of the lateralized (i.e., contralateral - ipsilateral) visual ERPs (e.g., the N1) and the CDA distributions. In doing so, we found a univariate outlier based on theta-based decoding measures (shown as an unfilled circle in Figure 9), and thus, the statistical results are reported excluding this data point.

## Results

### Experiment 1

#### Behavioral results

Behavioral performance at each set size was transformed into Cowan's K, using the formula K = set size x (hit rate – false alarm rate), separately for the short and long SOAs (Cowan, 2001). This allowed us to estimate the number of task-relevant colored squares represented in VWM at each set size. When the SOA between the cue and memory array was short, the mean K estimate was 0.9 (S.E. = 0.01), 1.7 (S.E. = 0.04), 2.1 (S.E. = 0.12), and 2.2 (S.E. = 0.17), for set sizes 1, 2, 4 and 8, respectively. For the long SOA conditions, the mean K estimate was 0.9 (S.E. = 0.02), 1.7 (S.E. = 0.04), 2.3 (S.E. = 0.12), and 1.8 (S.E. = 0.13), for set sizes 1, 2, 4, and 8, respectively. A repeated measures ANOVA showed that there was a main effect of set size due to the K estimate monotonically increasing up to set size 4, with no further increase for set size 8 ($F(1,19) = 26.9$, $p < .001$ for linear effect; $F(1,19) = 49.0$, $p < .001$ for quadratic effect). Planned comparisons further supported the observation that K only increased up to set size 4 ($t(19) = 9.6$, $p < .001$ for set size 1 versus 4, $t(19) = 3.6$, $p < .001$ for set size 2 versus 4, $t(19) = 0.6$ *n.s.* for set size 4 versus 8 in the short SOA conditions; $t(19) = 11.5$, $p < .001$

for set size 1 versus 4, $t(19) = 4.1$, $p < .01$ for set size 2 versus 4, $t(19) = -3.7$, $p < .001$ for set size 4 versus 8 in the long SOA conditions showing significantly smaller K estimate for set size 8 than 4). There was no main effect of SOA ($F(1,19) = 0.7$, *n.s.*), meaning that the participants were just as able to selectively remember the target items with both short and long SOAs. These results are in line with previously reported results utilizing bilateral change-detection tasks.

The CDA results

Figure 2 shows the difference waves between the contralateral and ipsilateral parieto-occiptical channels. The contralateral delay activity emerged 400 ms after the onset of the stimulus. The CDA monotonically increased up to set size 4 and reached a plateau for both short and long SOAs, revealing the classical capacity-defined set size function. The repeated measure ANOVA supported this observation with a significant effect of set size ($F(1,19) = 20.5$, $p < .001$ for linear effect, $F(1,19) = 10.3$, $p < .001$ for quadratic effect). Planned pairwise comparisons supported this observation ($t(19) = 4.8$, $ps < .001$ for set size 1 versus 4, $t(19) = 4.2$, $p < .001$ for set size 2 versus 4, $t(19) = -2.7$, $p = .01$, for set size 4 versus 8 in short SOA conditions, the CDA was smaller for set size 8 than set size 4; $t(19) = 6.7$, $p < .001$ for set size 1 versus 4, $t(19) = 4.1$, $p < .001$ for set size 2 versus 4, $t(19) = 0.6$, *n.s.* for set size 4 versus 8 in long SOA conditions). There also was a main effect of SOA ($F(1,19) = 6.5$, $p < .05$), but critically, there was no interaction between SOA and set size ($F(1,19) = 0.1$, n.s.). This suggested that although SOA influenced the overall amplitude of the CDA, it did not change the set size effect of the CDA. Thus, we observed the expected pattern of ERPs during this task in which spatially specific ERPs are measured contralateral to the remembered items. Next we turn to the question of whether the oscillatory activity of the EEG provides a measure of the spatially global representations that fMRI experiments suggest may exist.

Bilateral oscillations exhibit a set size function mirroring behavior

To determine whether spatially global VWM representations can be measured electrophysiologically we analyzed the frequency-band oscillations from electrodes that were contralateral and ipsilateral to the remembered objects. We found that the alpha-band activity (8-12Hz) was suppressed bilaterally. Moreover, as expected from a measure of VWM maintenance, this alpha suppression showed a set size function that changed in parallel with behavioral performance in the task. Figure 3 shows the event-related desynchronization for contralateral and ipsilateral parieto-occipital channels, separately. As can be seen, the capacity-limited set size function was observed across both contralateral and ipsilateral electrodes. That is, the event-related desynchronization of alpha monotonically increased up to set size 4 and reached the plateau for both sides in both SOA conditions. A repeated measures ANOVAs confirmed the presence of a significant effect of set size ($F(1,19) = 15.3$, $p = 0.001$ for linear effect, $F(1,19) = 5.6$, $p = .029$ for quadratic effect). Planned pairwise comparisons supported this observation ($ts(19) > 2.6$, $ps < .02$ for set size 1 versus 4, $ts(19) > 2.5$, $ps < .02$ for set size 2 versus 4, $ts(19) < 1.2$, *n.s.* for set size 4 versus 8 for the short SOA conditions; $ts(19) > 3.1$, $ps < .001$ for set size 1 versus 4, $ts(19) > 2.4$, $ps < .02$ for set size 2 versus 4, $ts(19) < 0.6$, *n.s.* for set size 4 versus 8 for the long SOA conditions). Critically, there was no main effect of laterality ($F(1,19) = 3.0$, *n.s.*) or interaction between set size and laterality ($F(1, 19) =$

1.2, *n.s.*). There was a main effect of SOA ($F(1,19) = 19.5$, $p < .001$), but this appears to reflect the neural response to the cue bleeding into the baseline activity for the short SOA conditions. Together, these results show that alpha-band activity has the defining characteristics of an electrophysiological index of spatially global VWM representations.

Next, we examined if the set size effect of parieto-occipital alpha power suppression exhibited contralateral bias during VWM maintenance. Figure 4 shows the difference waves between the contralateral and ipsilateral parieto-occipital alpha power suppression. A repeated measures ANOVA revealed that there was no main effect of set size ($Fs(1,19) < 2.5$, *n.s.*). This is in stark contrast with the CDA that shows a lateralized distribution, and thus, further supports the idea that this parieto-occipital alpha power suppression is a marker of spatially global VWM representations. In addition, Figure 4B shows that the lateralized desynchronization of alpha was most evident prior to the stimulus onset (long SOA trials) and the test item onset (short and long SOA trials). This suggests that the lateralized desynchronization of alpha indexes the orienting of attention in expectation of the upcoming event (Van Dijk et al., 2008, Handel et al., 2011, Haegens et al., 2012, Whitmarsh et al., 2014) rather than maintenance of VWM representations.

## Experiment 2

An alternative explanation for the ipsilateral desynchronization of alpha activity (8-12Hz) that we observed in Experiment 1 is that it indexes the suppression of the task-irrelevant items in the uncued hemifield (Sauseng et al., 2009). That is, instead of the bilateral alpha desynchronization being due to spatially global representations maintained in VWM, it is possible that ipsilateral desynchronizations show the characteristic set size function because the number of items in the task-irrelevant hemifield increased as the task-relevant set size increased. To dissociate the number of task-irrelevant objects from the number of task-relevant objects we manipulated the number of distractors presented independently of the number of task-relevant objects in the cued hemifield. If ipsilateral desynchronization of alpha is due to spatially global VWM representations, then we should see the capacity-defined set size function on ipsilateral channels regardless of the number of distractors. In contrast, if ipsilateral desynchronization of alpha is due to the suppression of distractors, then our distractor manipulation should destroy the ipsilateral set size function.

### Behavioral results

Similar to Experiment 1, behavioral performance was first converted to Cowan's K for each set size across the three different distractor conditions. In the matched distractor condition, the mean K estimates were 0.92 (S.E. = 0.01), 1.97 (S.E. = 0.14), and 1.68 (S.E. = 0.20) for set size 1, 4 and 8, respectively. In the one-distractor condition, the mean K estimates were 0.92 (S.E. = 0.01), 2.14 (S.E. = 0.15), and 2.03 (S.E. = 0.23) for set size 1, 4, and 8, respectively. In the eight-distractor condition, the mean K estimates were 0.92 (S.E. = 0.01), 2.05 (S.E. = 0.16), and 1.86 (S.E. = 0.19) for set size 1, 4, and 8, respectively. That is, the K estimate reached a plateau at set size 4 in all the distractor conditions. A repeated measures ANOVA for each distractor condition confirmed the main effects of set size ($Fs(1,19) > 14.7$ $p < .005$ for linear effect, $Fs(1,19)$

436 > 25.0, $p < .001$ for quadratic effect). Planned pairwise comparisons supported these
437 observations (*ts*(19) > 8.0 $p < .0001$ for set size 1 versus 4; *ts*(19) <1.2, *n.s.* for set size 4
438 versus 8 for one- and eight-distractor conditions and $t(19) = 2.3$, $p < .05$ for matched
439 distractor condition showing higher K for set size 4 than 8).
440
441 The CDA analysis
442 Figure 5 shows the difference waves (contralateral – ipsilateral parieto-occipital
443 responses) for each distractor condition. As can be seen, the CDA showed the capacity-
444 defined set size functions across all distractor conditions. That is, the CDA reached
445 asymptote at set size 4 in all distractor conditions. When the mean CDA amplitudes were
446 calculated as the mean amplitude from 400-1000 ms after the stimulus onset, and entered
447 into separate repeated measures ANOVA for each distractor condition, we found a
448 significant main effects of set size (*Fs*(1,19) > 22.0 $p < .005$ for linear effect, *Fs*(1,19) >
449 12.9, $p < .005$ for quadratic effect). Planned pairwise comparisons supported the
450 observation that the CDA increased from set size 1 to 4, but not from 4 to 8 (*ts*(19) > 4.8
451 $p < .001$ for set size 1 versus 4; *ts*(19) <1.9, *n.s.* for set size 4 versus 8). To better
452 examine the effect of distractors on the CDA, we ran an additional 2-way ANOVA
453 (factors of set size and distractor condition) excluding the matched distractor condition.
454 This revealed significant main effect of set size ($F(2, 38) = 32.9$, $p < .001$) as well as
455 distractor condition ($F(1, 19) = 16.5$, $p < .01$). Critically however, these two factors did
456 not interact ($F(2, 38) = 0.4$, n.s.). This suggests that our distractor load manipulation did
457 not affect the nature of the capacity-defined set size function of the CDA.
458
459 The spatially global alpha power suppression shows the capacity-defined set size effect
460 irrespective of the number of distractors.
461 We examined the sustained alpha power suppression (8-12Hz) to determine if it
462 shows the capacity-defined set size effect on both contralateral and ipsilateral electrodes
463 regardless of the number of the distractors. This should be the case if the spatially global
464 alpha power suppression truly indexes the spatially global VWM representations. As can
465 be seen in Figure 6, the sustained alpha power suppression reached an asymptote at set
466 size 4 across hemispheres in all distractor conditions. Repeated measures ANOVAs
467 statistically confirmed this observation (*Fs*(1,19)>5.6 , *ps* < .05 for linear effect, *Fs*(1,19)
468 > 7.5, *ps* < .03 for quadratic effects) as well as planned pairwise comparisons (*ts*(19) >
469 2.56, *ps* < .02 for set size 1 versus 4; *ts*(19) <1.5, *n.s.* for set size 4 versus 8 except for
470 ipsilateral channels in matched distractor condition $t(19) = 2.3$, $p < .05$ showing smaller
471 alpha power suppression for set size 8 than 4). Critically, there was no interaction
472 between set size and laterality (*Fs*(1,19) < 1, *n.s.* for linear effect, *Fs*(1,19) < 3.4, *n.s.* for
473 quadratic effect). To better examine the effect of distractors on the bilateral alpha power
474 suppression, we ran an additional 3-way ANOVA (with the factors of set size, distractor
475 condition, and laterality) excluding the matched distractor condition. The analysis
476 revealed a main effect of set size ($F(2,38) = 10.4$, $p < .001$) and laterality ($F(1,19) = 4.8$,
477 $p < .05$), but not distractor condition ($F(1,19) = 1.5$, n.s.). Once again, there was no
478 interaction across three factors (*F*s < 1, n.s.). This suggests that our distractor load
479 manipulation did not affect the nature of the capacity-defined set size function of the
480 spatially global alpha power suppression.
481

The lateralized alpha power suppression indexes orienting of attention

Similar to Experiment 1, we analyzed the lateralized alpha power suppression. In all the distractor conditions, the mean lateralized alpha power suppression amplitudes during the CDA interval (mean alpha power difference from 400-800ms after the stimulus onset) did not show the capacity-defined set size function ($Fs(1,19) < 1.6$, *n.s.* for linear effect, $Fs(1,19) < 2.2$, *n.s.* for quadratic effect except for the eight-distractor condition, $F(1,19) = 7.7$, $p < .05$). Figure 7 shows the lateralized alpha power suppression for each distractor condition. As can be seen, the lateralized alpha power suppression was most evident prior to the onset of the stimulus and the test item in all distractor conditions. These results replicated the results in Experiment 1 and further support the interpretation that the lateralized alpha power suppression indexes the orienting of attention in expectation of upcoming events, not the active maintenance of representations in visual working memory.

## Experiment 3

The goal of Experiment 3 was to determine if the contents of VWM can be decoded from the distribution of both the lateralized ERPs (i.e., the early sensory components and the CDA) and the spatially global oscillatory correlate of VWM (i.e., alpha power suppression). If these neural correlates truly index lateralized and spatially global VWM representations maintained in the brain, then it should be possible to use the scalp distribution of each signal during the retention interval to read out the contents of VWM using decoding analyses.

### Behavioral results

We examined the precision of subjects' behavioral report of the remembered orientation. Our dependent measure was the mean of the magnitude of response errors (i.e., the response offset in degrees from the orientation shown in the memory sample). The mean magnitude of the response offset was 5.6° (S.E. = 0.25). This indicates that subjects were able to maintain the target orientation with high precision.

### Decoding the content of VWM with the lateralized ERPs

Figure 8 shows the time course of the classification accuracy for VWM content using the scalp distribution of difference waves between channels that were contralateral and ipsilateral to the task-relevant hemifields. As can be seen, the content of VWM was reliably decoded during stimulus encoding and throughout the retention interval, whereas the distractor identity was not. To statistically evaluate the decoding performance, we calculated the mean decoding accuracy in a window from 100-400ms post-stimulus onset for the visual ERPs and 400-1000ms for the CDA. A separate repeated measures ANOVA revealed that there was a main effect of object identity for both visual ERPs ($F(1,23) = 18.7$, $p < .001$) and the CDA ($F(1,23) = 18.5$, $p < .001$), showing that the content of VWM was selectively decoded from the scalp distribution of the lateralized visual ERPs and the CDA. We then examined the pattern of errors that classifiers made (i.e., classification offsets). As can be seen from the distribution of classification offsets in Figure 8, the classification performance had a graded profile. This shows that when the

classifiers made errors, they tended to choose nearby orientations over more distant ones (Brouwer and Heeger, 2009, Ester et al., 2013).

We also examined if content of VWM can be decoded from small but systematic eye movements (Figure 8). The results of the decoding analysis using the EOG channels (VEOG and HEOG channels) revealed that this was not the case. More precisely, the classification accuracy for the VWM content (i.e., cued item) fluctuated around chance level throughout the retention interval, and it was not significantly above chance in any time window (*p*s >.05).

Decoding the content of VWM with alpha oscillations

Figure 8 shows the time course of the classification accuracy for both contralateral and ipsilateral alpha power (8-12 Hz). As can be seen, the content of VWM was reliably decoded from both the contralateral and ipsilateral scalp distributions of alpha power, and that this was sustained across the retention interval. Critically, these scalp distributions of alpha power consistently failed to decode the distractor orientation throughout the retention interval. To provide statistical support for these observations, we calculated mean classification accuracy from 400-1000ms after the stimulus onset. A 2-way repeated measures ANOVA revealed a significant main effect of object identity (i.e., target versus distractor, $F(1,23) = 13.5$, $p < .01$) but no main effect of laterality (i.e., contralateral versus ipsilateral, $F(1,23) = .37$, n.s.) nor interaction between object identity and laterality ($F(1,23) = .74$, n.s.). That is, the target orientation was reliably decoded by both contralateral and ipsilateral scalp distributions of alpha power, but the distractor orientation was not.

As can be seen from the distribution of classification offsets, the classification performance had a graded profile showing that when the classifiers made errors, they tended to choose nearby orientations over more distant ones (Brouwer and Heeger, 2009, Ester et al., 2013). Critically, contralateral and ipsilateral scalp distributions of alpha power were equally good at decoding the content of VWM ($F(7,161) = 0.2$, n.s. for the main effect of laterality, and $F(7,161) = 0.58$, n.s. for interaction between laterality and offset). These results directly support the hypothesis that bilateral alpha desychronization provides an index of VWM representations.

Finally, to validate that the VWM decodablity is the result of spatially global VWM representations but not of two independent hemisphere-specific VWM representations, we examined if accurate outputs of contralateral and ipsilateral decoders are temporally synchronized. Here, we found that the probability that both contralateral and ipsilateral decoders output accurate responses was statistically higher than the chance level estimated under the assumption that contralateral and ipsilateral decoders made independent predictions ($t(23) =8.4$, $p < .001$). This buttresses our claim that the bilateral alpha power signal reflects the existence of spatially global VWM representations.

The decoding analysis also showed a transient response in the theta band (4-7Hz) power that appears to encode the stimuli. Figure 9 shows the time course of the classification accuracy from this parieto-occipital theta activity. As can be seen, the ipsilateral and contralateral distribution of theta power in the time window from 100-400ms after stimulus onset reliably classified stimulus identity. Interestingly, distractor orientation was also decodable from the contralateral theta power to distractor side (i.e. ipsilateral to target) ($t(23) = 3.0$, $p < .01$) but not from ipsilateral theta power. A repeated

measures ANOVA confirmed this observation by showing that there was a main effect of object identity (i.e., Target versus Distractor, $F(1, 23) = 9.0$, $p < .01$) and a main effect of laterality (i.e., Contralateral versus Ipsilateral, $F(1, 23) = 12.0$, $p < .01$), but no interaction ($F(1, 23) = 0.9$ , n.s.). The fact that the theta response was transient, however, questions its validity as a neural correlate of storage in VWM because it did not continue through the retention interval. Instead, its transient nature makes it a great candidate for a neural correlate of stimulus encoding, which we will discuss below.

Relationship between lateralized and spatially global VWM representations

Next, we examined the relationships among the neural measures of VWM. If spatially global VWM representations truly exist, then the quality of contralateral and ipsilateral read-out of such representations should be correlated. In other words, we would expect that those who show high contralateral decodability should also show high ipsilateral decodability. As Figure 10 shows, this was precisely the case. For alpha-based decoding, those who showed higher contralateral decoding accuracy showed higher ipsilateral decoding accuracy ($r = .47$, $p < .05$). Interestingly, the decoding performance using the spatially global oscillatory activity was not related to performance using lateralized activity observed at the same time scale. That is, the CDA-based decoding performance was not correlated with contralateral nor ipsilateral alpha-based decoding performance ($rs < .16$, n.s.). Importantly, this lack of correlation between the CDA-based decoding performance and alpha-based decoding performance was not due to unreliable measurement of the CDA-based decoding performance because the CDA-based decoding showed a reliable relationship with decoding performance using the early visual ERPs (from 100-400ms post-stimulus)($r =. 50$, $p < .05$). This is consistent with the idea that there exist lateralized and spatially global VWM representations that are dissociable (Fukuda et al., 2015).

Interestingly however, neural measures observed during perceptual encoding showed some interrelations. Theta-based decoding performance was correlated across hemispheres ($r = .49$, $p < .05$), showing its spatially global nature of perceptual encoding. When correlated with decoding performance using the early visual ERPs, the contralateral decoding revealed a significant relationship ($r = .51$, $p < .05$), where as ipsilateral decoding did not ($r = .13$, n.s.). This makes sense given the contralateral bias for theta-based decoding and the more robust distractor representation in the ipsilateral theta distribution. Together, this is consistent with the idea that theta power response at least partially reflects the initial volley of sensory activity in the visual system that generates the early visual ERPs (e.g., the visual N1).

## Discussion

In this study, we sought to understand the relationship between neuroimaging and electrophysiological findings about the spatial nature of VWM representations. In Experiment 1 and 2, we used the hallmark of VWM capacity limitations, the increase in the number of objects remembered up to an asymptote, to identify both spatially specific and spatially global VWM representations. We reasoned that the electrophysiological activity underlying the representation of objects in VWM should increase monotonically up to the capacity limit of VWM and remain at that level even at higher set sizes. As

expected, the spatially specific CDA demonstrated this capacity-defined set size effect. However, we also found a spatially global electrophysiological signal that showed this same capacity limit. Specifically, we found bilateral alpha-band desychronization that changed in magnitude with additional items in memory, until VWM capacity was reached. Finally, the scalp distribution of this spatially global alpha power suppression in either hemisphere, as well as that of the CDA, was sufficient to read out the object represented in VWM. These results indicate that both spatially specific and spatially global VWM representations are maintained in the brain and they can be measured simultaneously.

One remaining question is what exactly it is that the scalp distribution of the CDA and the alpha power decoded in Experiment 3. Although we asked participants to remember the orientation of the bars, presumably by storing this object representation in VWM, participants could have simply kept their attention on where the bar met the ring. The present study does not allow us to distinguish between these alternative explanations of the effects. One major difficulty in making such a distinction is the intricate relationship between the definition of spatial working memory and sustained spatial attention (Chun, 2011). Foster and colleagues (2016) have recently attempted this dissociation by differentiating the stimulus location and the location at which participants reported the stimulus. Indeed, they successfully showed that the scalp distribution of alpha power decoded the stimulus location even in a task in which participants reported all different stimulus locations at a single test location. Although this result seems to indicate that the scalp distribution of alpha power is related to working memory rather than the locus of spatial attention, future studies are necessary to come to a definitive conclusion.

Selective maintenance of spatially global VWM representations

Our study provides novel findings about the nature of the spatially global VWM representations. In previous fMRI studies in which the content of VWM was successfully decoded from patterns of muti-voxel activity, the target stimulus was either presented in isolation or with another target item (Ester et al., 2009, Pratte and Tong, 2014). Thus, it was unclear if a spatially global representation is constructed for any visually presented object without regard to its task relevance.

Our study tested for effects of task relevance by simultaneously presenting a distractor. The finding that neither contralateral nor ipsilateral scalp distribution of alpha power reliably decoded the distractor identity supports the selectivity of this spatially global VWM activity for the items that are being held in memory. Although there was a bias toward the target item, the transient contralateral theta power distribution reliably classified the identity of both target and distractor representations. This suggests that the distractor information was perceptually encoded but was not maintained in VWM over the retention interval. It would be interesting for a future study to examine the difference in these neighboring frequency responses. For example, why was the distractor item was decodable from the transient contralateral theta power response? One hypothesis is that this theta response reflects the automatic perceptual encoding of visual stimuli, and top-down mechanisms act on this automatic processing to bias the maintenance of the target item over the distractor item. Another hypothesis is that this theta response is under voluntary control and underlies the selective encoding of the target item on a majority of

the trials, but subjects erroneously encoded the distractor item and then removed it from VWM on a small number of trials due to occasional lapses of attention (Adam et al., 2015). As a consequence, the transient theta power response reflects the distractor items, and thus, is sensitive to the identity of the distractor. Future work focused on this oscillatory signature will be needed to distinguish between these hypotheses that fall out of the present study.

Dissociable correlates of two types of VWM representations

Our study showed that electrophysiological correlates of the contralateral and the spatially global VWM representations are dissociable. The existence of the two types of VWM representations could explain the contralateral superiority in multi-voxel pattern (MVP) classification to decode the content of VWM. In Pratte and Tong (2014), they found that contralateral MVP in primary visual areas classified the content of VWM significantly better than its ipsilateral counterpart. Given that the contralateral hemisphere has both spatially specific and the spatially global VWM representations, it is reasonable that the contralateral MVP can classify the content of VWM better than the ipsilateral MVP.

The discovery of dissociable neural correlates for contralateral and spatially global VWM will lead to a more precise characterization of VWM as well as its relationship with other cognitive abilities. Recently, many studies have utilized the ERP correlate of the contralateral VWM representation (i.e., the CDA) to infer the nature of VWM representation and its relationship with other cognitive abilities (Vogel et al., 2005, Fukuda and Vogel, 2009, Luria and Vogel, 2011, Spronk et al., 2013, Tsubomi et al., 2013, Unsworth et al., 2014b, Reinhart and Woodman, 2015). It will be interesting to examine the similarities and differences that our spatially global VWM representations exhibit compared to the lateralized representations, since the comparison may result in a more holistic understanding of VWM and how it is used in complex cognitive processing.

Acknowledgements

This research was supported by the National Eye Institute of the National Institutes of Health (R01-EY019882, R01-EY025275, P30-EY08126, and T32-EY007135).

References

Adam KC, Mance I, Fukuda K, Vogel EK (2015) The Contribution of Attentional Lapses to Individual Differences in Visual Working Memory Capacity. Journal of cognitive neuroscience 1-16.

Brouwer GJ, Heeger DJ (2009) Decoding and reconstructing color from responses in human visual cortex. The Journal of neuroscience : the official journal of the Society for Neuroscience 29:13992-14003.

Chun MM (2011) Visual working memory as visual attention sustained internally over time. Neuropsychologia 49:1407-1409.

Cowan N (2001) The magical number 4 in short-term memory: a reconsideration of mental storage capacity. The Behavioral and brain sciences 24:87-114; discussion 114-185.

Ester EF, Anderson DE, Serences JT, Awh E (2013) A neural measure of precision in visual working memory. Journal of cognitive neuroscience 25:754-761.

Ester EF, Serences JT, Awh E (2009) Spatially global representations in human primary visual cortex during working memory maintenance. The Journal of neuroscience : the official journal of the Society for Neuroscience 29:15258-15265.

Foster JJ, Sutterer DW, Serences JT, Vogel EK, Awh E (2016) The topography of alpha-band activity tracks the content of spatial working memory. Journal of neurophysiology 115:168-177.

Fukuda K, Mance I, Vogel EK (2015) alpha Power Modulation and Event-Related Slow Wave Provide Dissociable Correlates of Visual Working Memory. The Journal of neuroscience : the official journal of the Society for Neuroscience 35:14009-14016.

Fukuda K, Vogel E, Mayr U, Awh E (2010) Quantity, not quality: the relationship between fluid intelligence and working memory capacity. Psychonomic bulletin & review 17:673-679.

Fukuda K, Vogel EK (2009) Human variation in overriding attentional capture. The Journal of neuroscience : the official journal of the Society for Neuroscience 29:8726-8733.

Haegens S, Luther L, Jensen O (2012) Somatosensory anticipatory alpha activity increases to suppress distracting input. Journal of cognitive neuroscience 24:677-685.

Handel BF, Haarmeier T, Jensen O (2011) Alpha oscillations correlate with the successful inhibition of unattended stimuli. Journal of cognitive neuroscience 23:2494-2502.

Harrison SA, Tong F (2009) Decoding reveals the contents of visual working memory in early visual areas. Nature 458:632-635.

Luria R, Vogel EK (2011) Visual search demands dictate reliance on working memory storage. The Journal of neuroscience : the official journal of the Society for Neuroscience 31:6199-6207.

Pratte MS, Tong F (2014) Spatial specificity of working memory representations in the early visual cortex. Journal of vision 14:22.

747 Reinhart RM, Woodman GF (2015) Enhancing long-term memory with stimulation
748 tunes visual attention in one trial. Proceedings of the National Academy of
749 Sciences of the United States of America 112:625-630.
750 Sauseng P, Klimesch W, Heise KF, Gruber WR, Holz E, Karim AA, Glennon M, Gerloff
751 C, Birbaumer N, Hummel FC (2009) Brain Oscillatory Substrates of Visual
752 Short-Term Memory Capacity. Current Biology 19:1846-1852.
753 Serences JT, Ester EF, Vogel EK, Awh E (2009) Stimulus-specific delay activity in
754 human primary visual cortex. Psychological science 20:207-214.
755 Spronk M, Vogel EK, Jonkman LM (2013) No behavioral or ERP evidence for a
756 developmental lag in visual working memory capacity or filtering in
757 adolescents and adults with ADHD. PloS one 8:e62673.
758 Tsubomi H, Fukuda K, Watanabe K, Vogel EK (2013) Neural limits to representing
759 objects still within view. The Journal of neuroscience : the official journal of
760 the Society for Neuroscience 33:8257-8263.
761 Unsworth N, Fukuda K, Awh E, Vogel EK (2014a) Working memory and fluid
762 intelligence: capacity, attention control, and secondary memory retrieval.
763 Cognitive psychology 71:1-26.
764 Unsworth N, Fukuda K, Awh E, Vogel EK (2014b) Working Memory Delay Activity
765 Predicts Individual Differences in Cognitive Abilities. Journal of cognitive
766 neuroscience 1-13.
767 Van Dijk H, Schoffelen JM, Oostenveld R, Jensen O (2008) Prestimulus oscillatory
768 activity in the alpha band predicts visual discrimination ability. Journal of
769 Neuroscience 28:1816-1823.
770 Vogel EK, Machizawa MG (2004) Neural activity predicts individual differences in
771 visual working memory capacity. Nature 428:748-751.
772 Vogel EK, McCollough AW, Machizawa MG (2005) Neural measures reveal individual
773 differences in controlling access to working memory. Nature 438:500-503.
774 Whitmarsh S, Barendregt H, Schoffelen JM, Jensen O (2014) Metacognitive
775 awareness of covert somatosensory attention corresponds to contralateral
776 alpha power. NeuroImage 85 Pt 2:803-809.
777
778

Figure Captions

Figure 1. The procedures of the bilateral VWM tasks used in the present study. The top panel shows the color change-detection task used in Experiment 1 (and Experiment 2, with the number of objects in the distractor array manipulated). The bottom panel shows the orientation recall task used in Experiment 3.

Figure 2. The CDA results from Experiment 1. The top panel shows the results from the short SOA condition and the bottom shows the results from the long SOA condition. The waveforms are the difference waves for each set size, and the time windows for the stimulus events (dark gray region for the cue, marked *Cue*, light gray region for the memory array, marked *Stim*) and the CDA (magenta region) are highlighted. The bar graphs show the mean CDA amplitudes for each set size. The error bars on bar graphs represent S.E.M., and the asterisks represent the results of planned t-tests (* = <.05, ** = <.01, *** = <.001).

Figure 3. The sustained alpha power suppression measured in Experiment 1. Top panels show the contralateral (left) and the ipsilateral (right) alpha power suppression for short SOA conditions. The bottom panels show the same for the long SOA conditions. The time windows for the stimulus onset and the sustained alpha power suppression are highlighted as in Figure 2 (with the alpha suppression window shown in magenta). The error bars on bar graphs represent S.E.M., and the asterisks represent the results of planned t-tests (* = <.05, ** = <.01).

Figure 4. The contralateral alpha power suppression measured in Experiment 1. Panel A) The results from the short SOA condition (top) and long SOA condition (bottom). The waveforms are the difference waves for each set size, and the time windows for the stimulus events and the CDA are highlighted as in Figure 2. Note that the time points along the x-axis indicate the center of the 400ms time window. The bar graphs show the mean alpha power suppression during the CDA time-window for each set size. Panel B) The time course of the contralateral alpha power suppression for short and long SOA conditions averaged across all set sizes. The error bars represent S.E.M.

Figure 5. The CDA and contralateral alpha power suppression measured in Experiment 2. This figure shows the CDA results for matched distractor (top), one-distractor (middle), and eight-distractor (bottom) conditions. The waveforms are the difference waves for each set size, and the time windows for the stimulus event and the CDA are highlighted accordingly. The bar graphs show the mean CDA amplitudes during the highlighted window for each set size. The error bars on bar graphs represent S.E.M., and the asterisks represent the results of planned t-tests (*** = <.001).

Figure 6. The sustained alpha power suppression measured in Experiment 2.

Top panel shows the contralateral (left) and the ipsilateral (right) alpha power suppression for matched distractor conditions. The middle panels show the same for one-distractor condition, and the bottom does for the eightdistractor condition. The time windows for the stimulus onset and the sustained alpha power suppression are highlighted accordingly. The bar graphs show the mean alpha power for each set size. The error bars represent S.E.M. The error bars on bar graphs represent S.E.M., and the asterisks represent the results of planned t-tests (* = <.05, ** = <.01).

Figure 7. The Contralateral alpha power suppression measured in Experiment 2.
Panel A) The lateralized alpha power suppression for matched distractor (top), one-distractor (middle), and eight-distractor (bottom) conditions. The waveforms are the difference waves (contralateral - ipsilateral) for each set size, and the time windows for the stimulus event and the CDA are highlighted accordingly. The bar graphs show the mean lateralized alpha power suppression during the CDA window for each set size. Panel B) The time course of the contralateral alpha power suppression for matched, one-distractor, and eight-distractor conditions averaged across all set sizes. The events and time windows are highlighted as in Panel A (with the addition of the test stimulus presentation shown in turquoise). The error bars on bar graphs represent S.E.M.

Figure 8. The ERP-based classification results from Experiment 3.
Top left and bottom left panels show the classification accuracy for the target (red) and distractor (blue) using the scalp distribution of the difference waves (i.e., contralateral-ipsilateral amplitudes) and EOG channels, respectively. Note that the laterality was defined with respect to the cued hemifield. The solid black line indicates the chance level of classification. The top right and bottom right panels show the distribution of response offsets produced by the VEPs-based decoder and the CDA-based decoder, respectively. The red lines show the result for target decoding, and the blue lines show that for distractor decoding. The error bars represent S.E.M.

Figure 9. The oscillation-based classification results from Experiment 3.
Panel A) The results of the classification analyses based on the scalp distribution of alpha (8-12Hz) power. The top left figure shows the classification accuracy for target item using the scalp distribution of the contralateral (red) and ipsilateral (magenta) alpha power. The bottom left show the classification accuracy for distractor item based on contralateral (blue) and ipsilateral (cyan) alpha power distribution. Note that the laterality was defined with respect to the item of interest. The solid black line indicates the chance level of classification. The line graph on the left shows the distribution of response offsets produced by the alpha-power-based decoders. The red (contralateral) and magenta (ipsilateral) lines show the result for target decoding, and the blue (contralateral) and cyan (ipsilateral) lines show that for distractor decoding. The error bars represent S.E.M.
Panel B) The results of the classification analyses based on the scalp distribution of theta (4-7Hz) power. The top left figure shows the classification accuracy for target item using the scalp distribution of the contralateral (red) and ipsilateral (magenta) theta power. The bottom left show the classification accuracy for distractor item based on contralateral

(blue) and ipsilateral (cyan) theta power distribution. Note that the laterality was defined with respect to the item of interest. The solid black line indicates the chance level of classification. The line graph on the left shows the distribution of response offsets produced by the theta-power-based decoders. The red (contralateral) and magenta (ipsilateral) lines show the result for target decoding, and the blue (contralateral) and cyan (ipsilateral) lines show that for distractor decoding. The error bars represent S.E.M.

Figure 10. The results of correlational analyses from Experiment 3.
Panel A) Correlations between neural correlates of spatially global and lateralized VWM representations. The left scatter plot shows the correlation between decoding accuracies based on the scalp distributions of contralateral and ipsilateral alpha (8-12Hz) power. The right two scatter plots show the relationship between the decoding accuracies between the CDA-based and the contralateral alpha-power-based decoders (red) and between the CDA-based and the ipsilateral alpha-power-based decoders (blue). Panel B) Correlations between neural correlates of perceptual encoding. The left scatter plot shows the correlation between decoding accuracies based on the scalp distributions of contralateral and ipsilateral theta (4-7Hz) power. The right two scatter plots show the relationship between the decoding accuracies between the VEPs-based and the contralateral theta-power-based decoders (red) and between the VEPs-based and the ipsilateral theta-power-based decoders (blue). Panel C) The correlation between VEPs-based decoding performance and the CDA-based decoding performance. The asterisks represent the statistical significance of correlations (* = <.05).

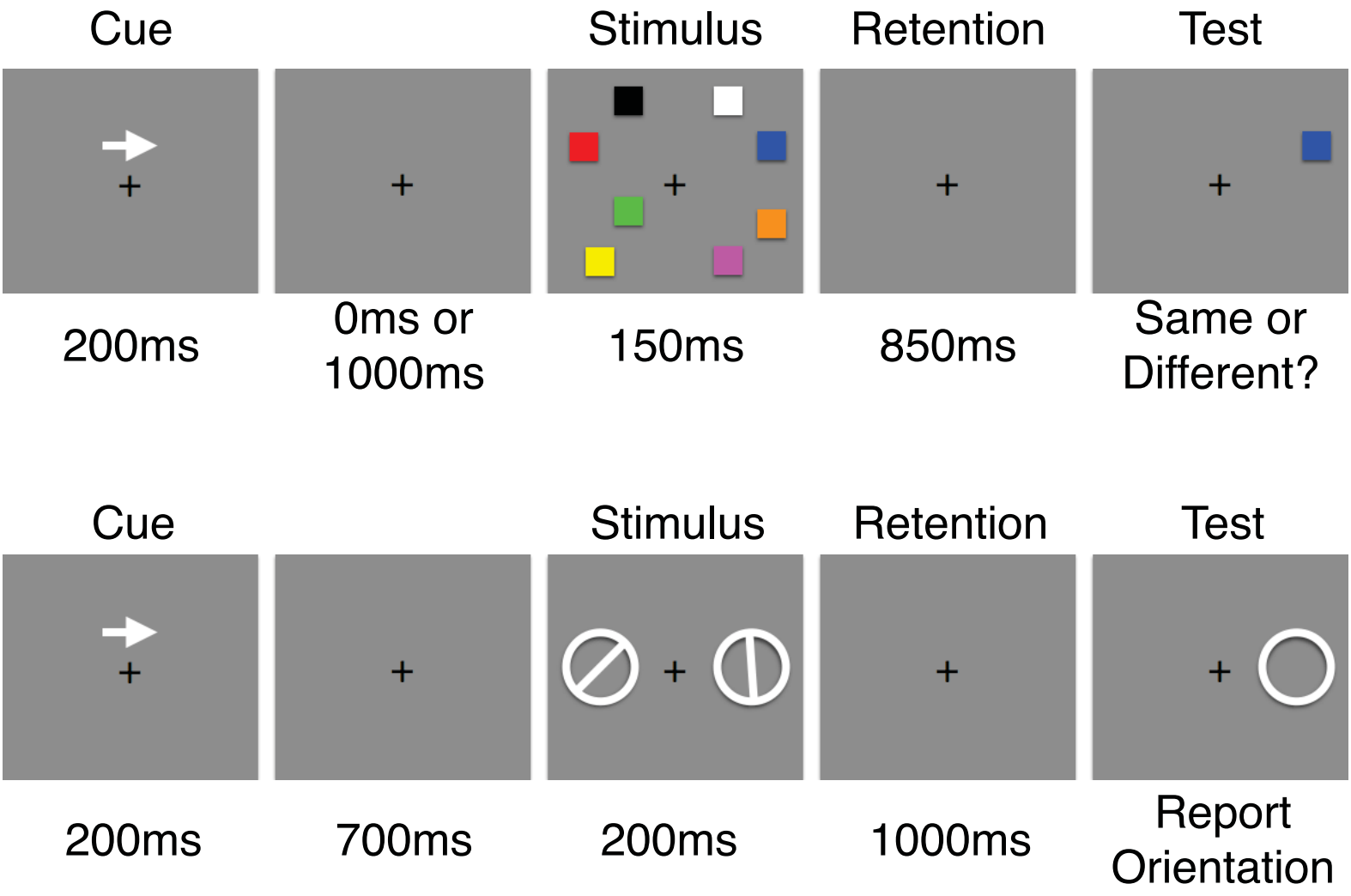


Figure 1. The procedures of the bilateral VWM tasks used in the present study. The top panel shows the color change-detection task used in Experiment 1 (and Experiment 2, with the number of objects in the distractor array manipulated). The bottom panel shows the orientation recall task used in Experiment 3.

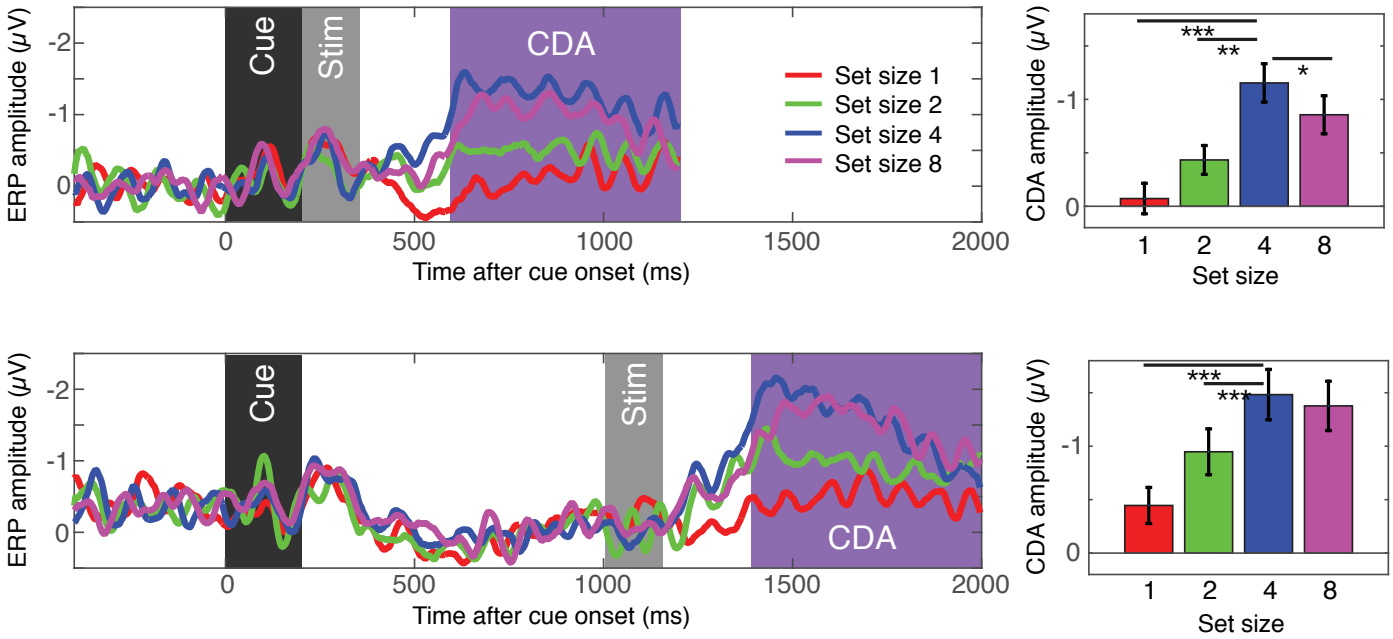


Figure 2. The CDA results from Experiment 1. The top panel shows the results from the short SOA condition and the bottom shows the results from the long SOA condition. The waveforms are the difference waves for each set-size, and the time windows for the stimulus events (dark gray region for the cue, marked Cue, light gray region for the memory array, marked Stim) and the CDA (magenta region) are highlighted. The bar graphs show the mean CDA amplitudes for each set size. The error bars on bar graphs represent S.E.M., and the asterisks represent the results of planned t-tests (* = <.05, ** = <.01, *** = <.001).

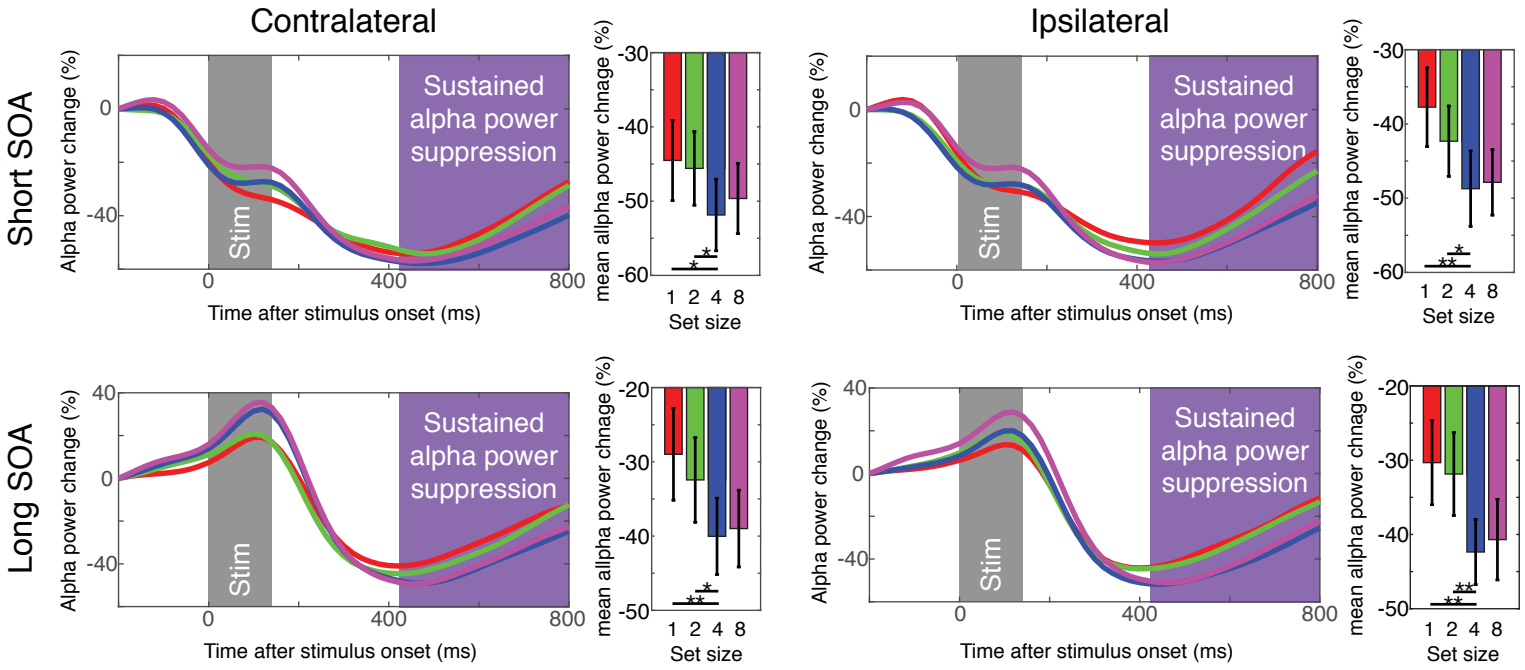


Figure 3. The sustained alpha power suppression in Experiment 1.
Top panels show the contralateral (left) and the ipsilateral (right) alpha power suppression for short SOA conditions. The bottom panels show the same for the long SOA conditions. The time windows for the stimulus onset and the sustained alpha power suppression are highlighted as in Figure 2 (with the alpha suppression window shown in magenta). The error bars on bar graphs represent S.E.M., and the asterisks represent the results of planned t-tests (* = <.05, ** = <.01).

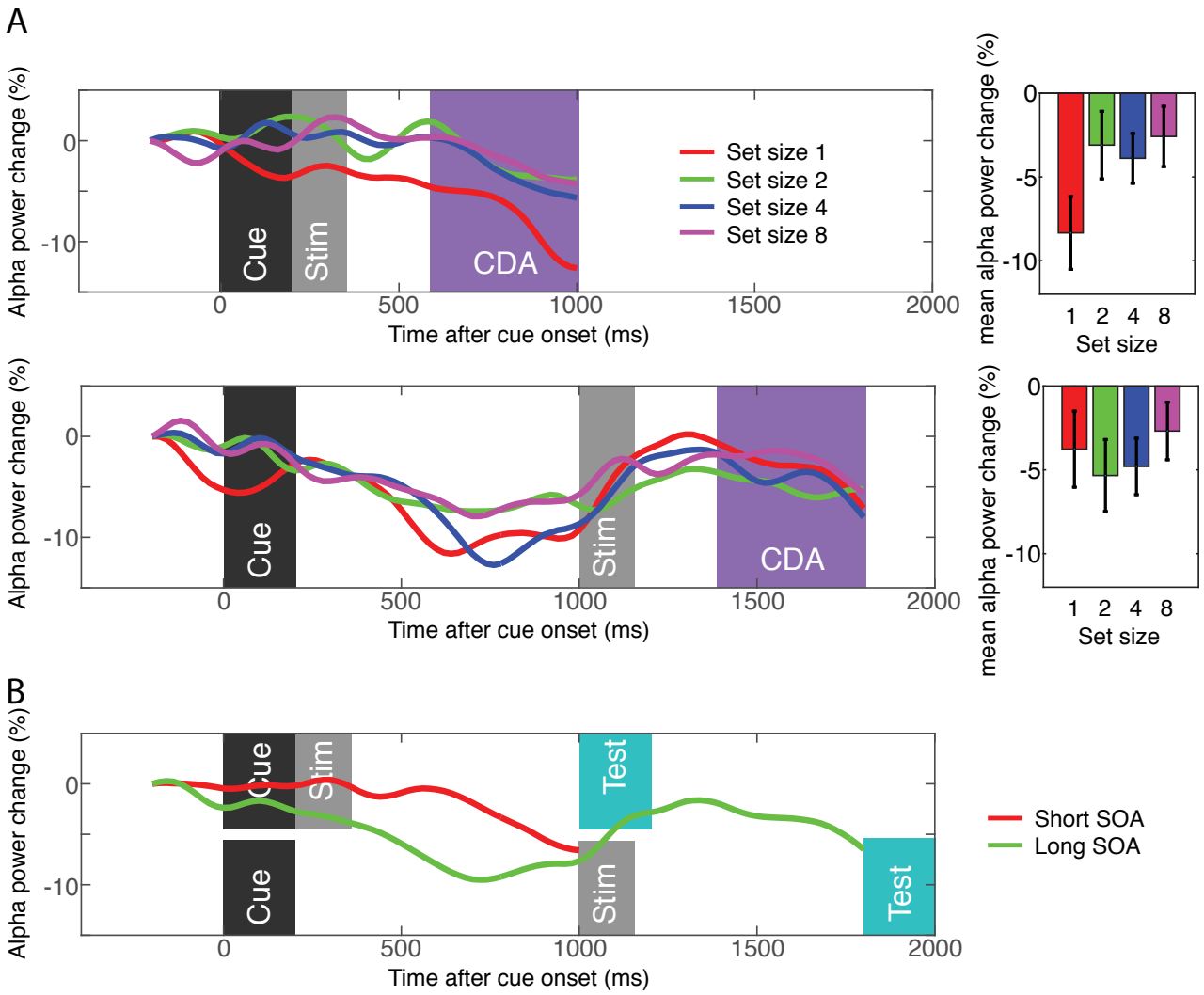


Figure 4. The lateralized alpha power suppression measured in Experiment 1.
Panel A) The results from the short SOA condition (top) and long SOA condition (bottom). The waveforms are the difference waves (contralateral - ipsilateral) for each set size, and the time windows for the stimulus events and the CDA are highlighted as in Figure 2. Note that the time points along the x-axis indicate the center of the 400ms time window. The bar graphs show the mean alpha power suppression during the CDA time-window for each set size. Panel B) The time course of the contralateral alpha power suppression for short and long SOA conditions averaged across all set sizes. The error bars represent S.E.M.

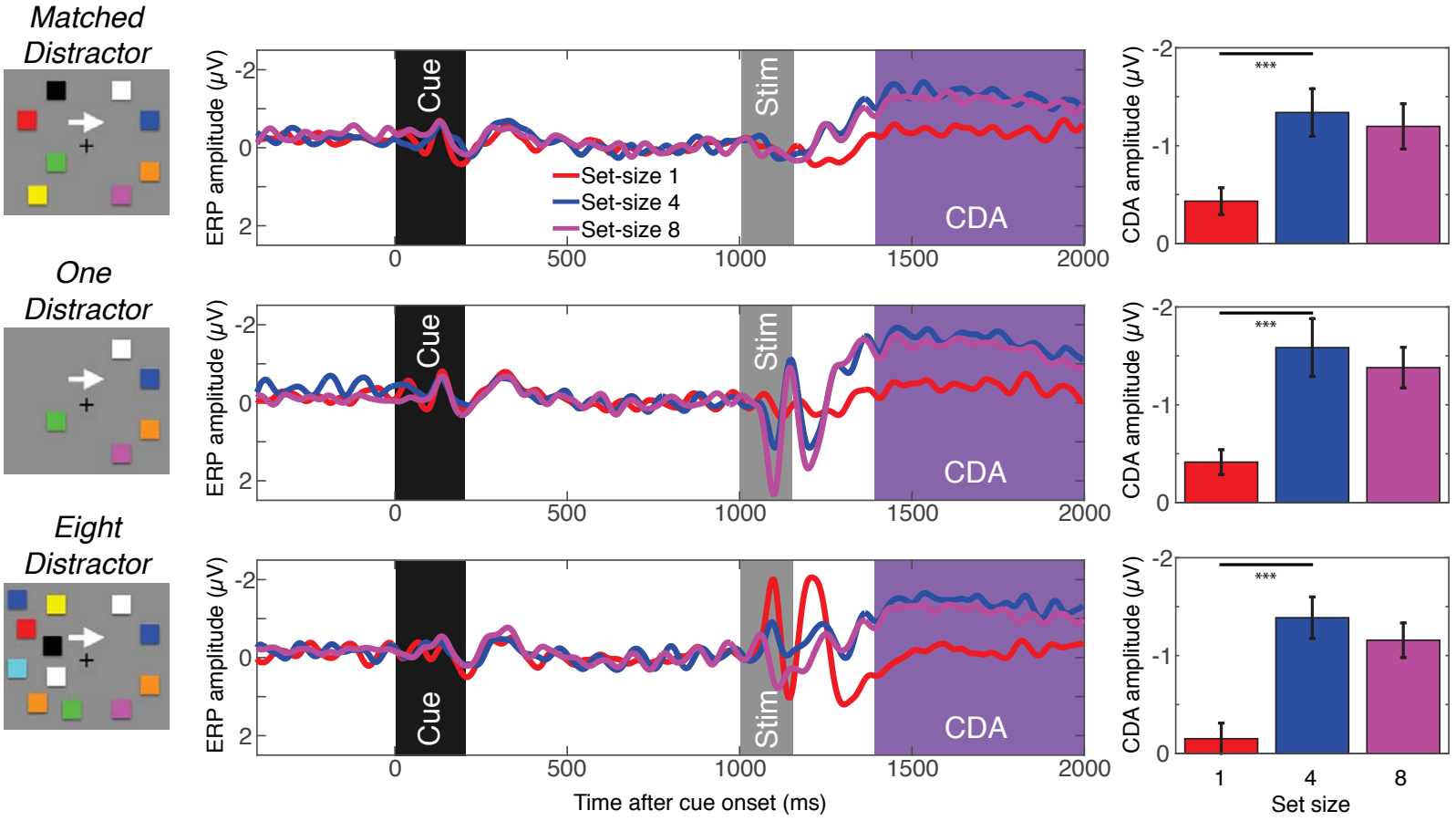


Figure 5. The CDA measured in Experiment 2.
This figure shows the CDA results for matched distractor (top), one-distractor (middle), and eight-distractor (bottom) conditions. The waveforms are the difference waves for each set size, and the time windows for the stimulus event and the CDA are highlighted accordingly. The bar graphs show the mean CDA amplitudes during the highlighted window for each set size. The error bars on bar graphs represent S.E.M., and the asterisks represent the results of planned t-tests (*** = <.001).

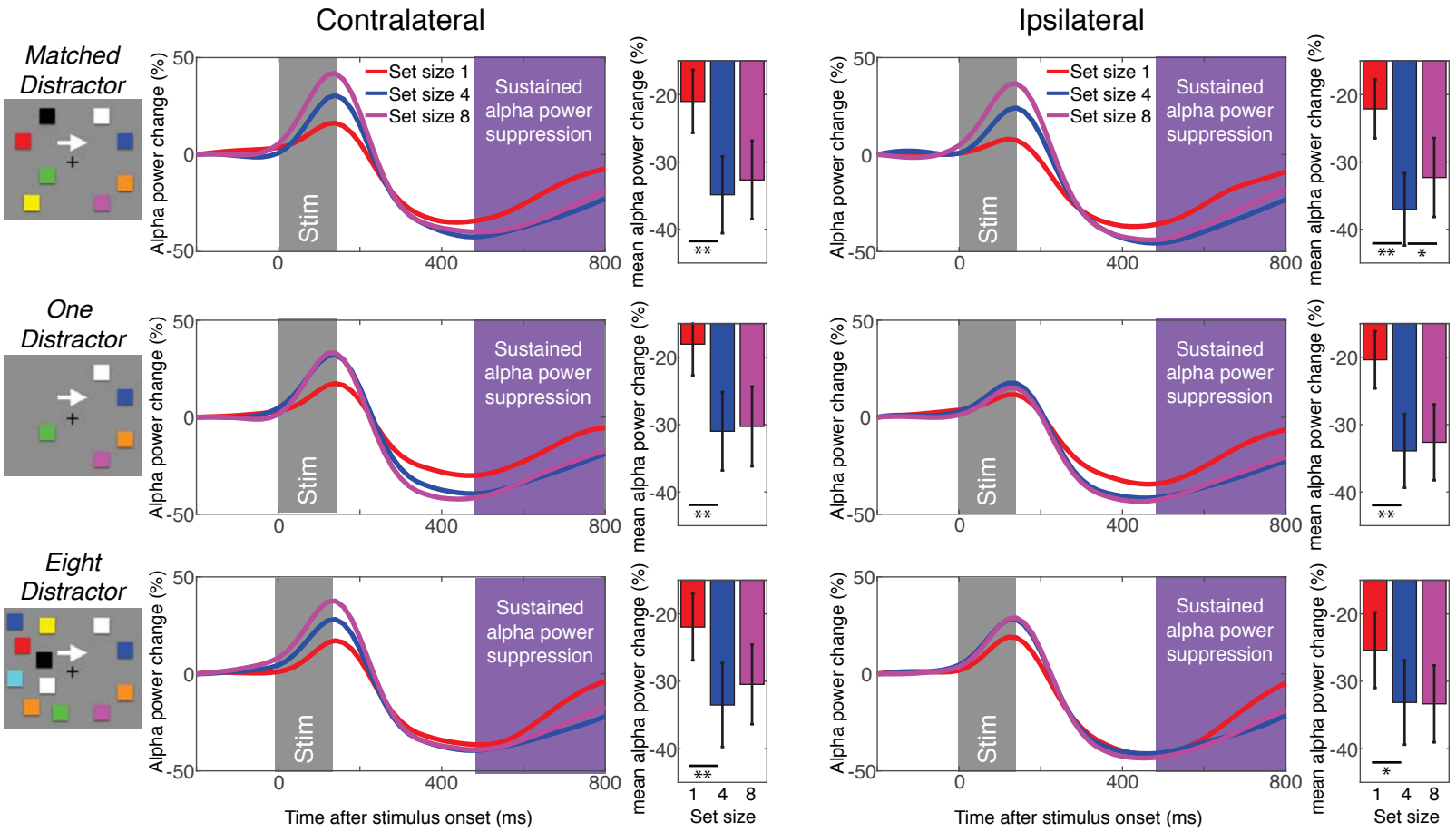


Figure 6. The sustained alpha power suppression measured in Experiment 2.
Top panel shows the contralateral (left) and the ipsilateral (right) alpha power suppression for matched distractor conditions. The middle panels show the same for one-distractor condition, and the bottom does for the eight-distractor condition. The time windows for the stimulus onset and the sustained alpha power suppression are highlighted accordingly. The bar graphs show the mean alpha power for each set size. The error bars represent S.E.M. The error bars on bar graphs represent S.E.M., and the asterisks represent the results of planned t-tests (* = <.05, ** = <.01).

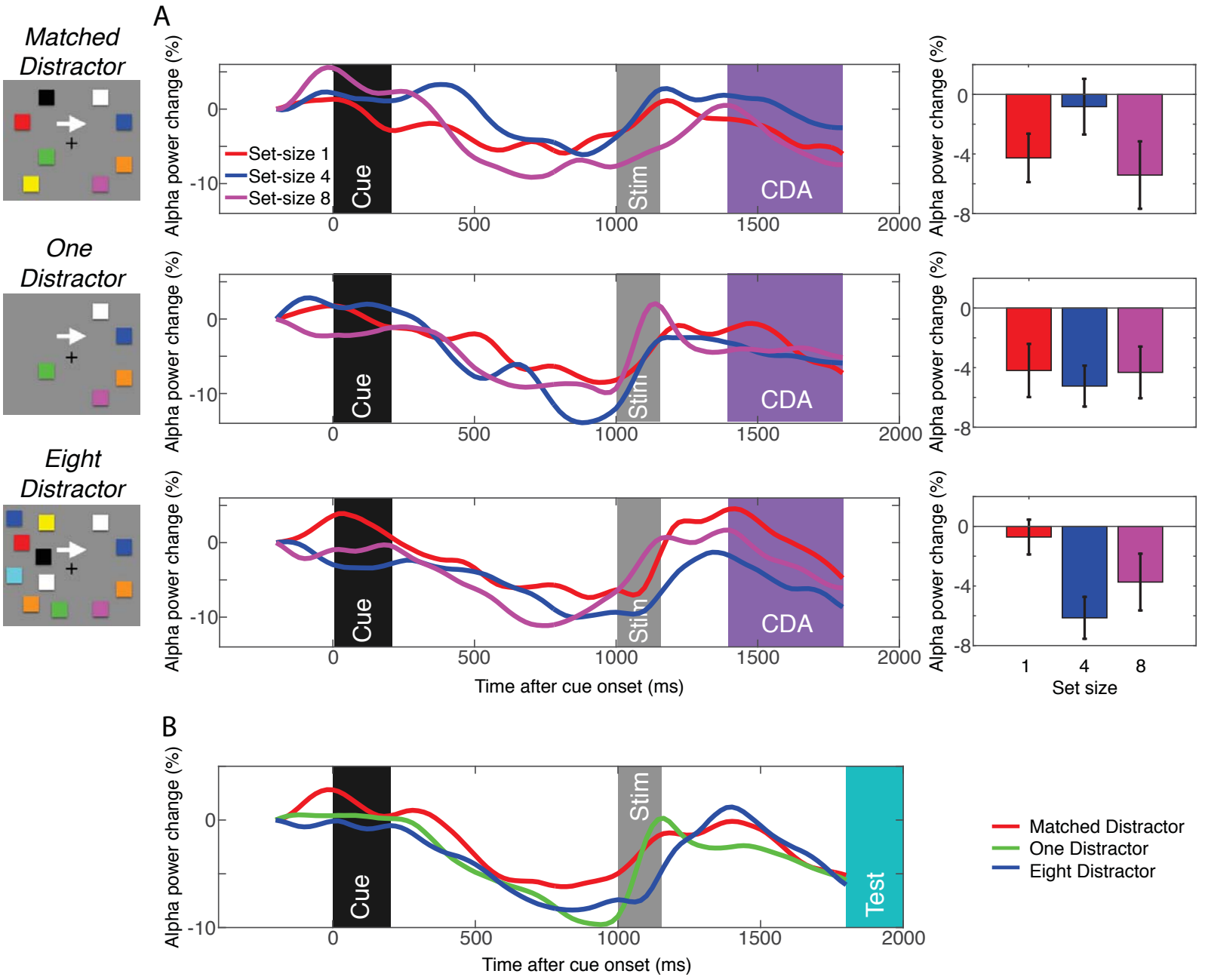


Figure 7. The Contralateral alpha power suppression measured in Experiment 2.
Panel A) The lateralized alpha power suppression for matched distractor (top), one-distractor (middle), and eight-distractor (bottom) conditions. The waveforms are the difference waves (contralateral - ipsilateral) for each set size, and the time windows for the stimulus event and the CDA are highlighted accordingly. The bar graphs show the mean lateralized alpha power suppression during the CDA window for each set size. Panel B) The time course of the contralateral alpha power suppression for matched, one-distractor, and eight-distractor conditions averaged across all set sizes. The events and time windows are highlighted as in Panel A (with the addition of the test stimulus presentation shown in turquoise). The error bars on bar graphs represent S.E.M.

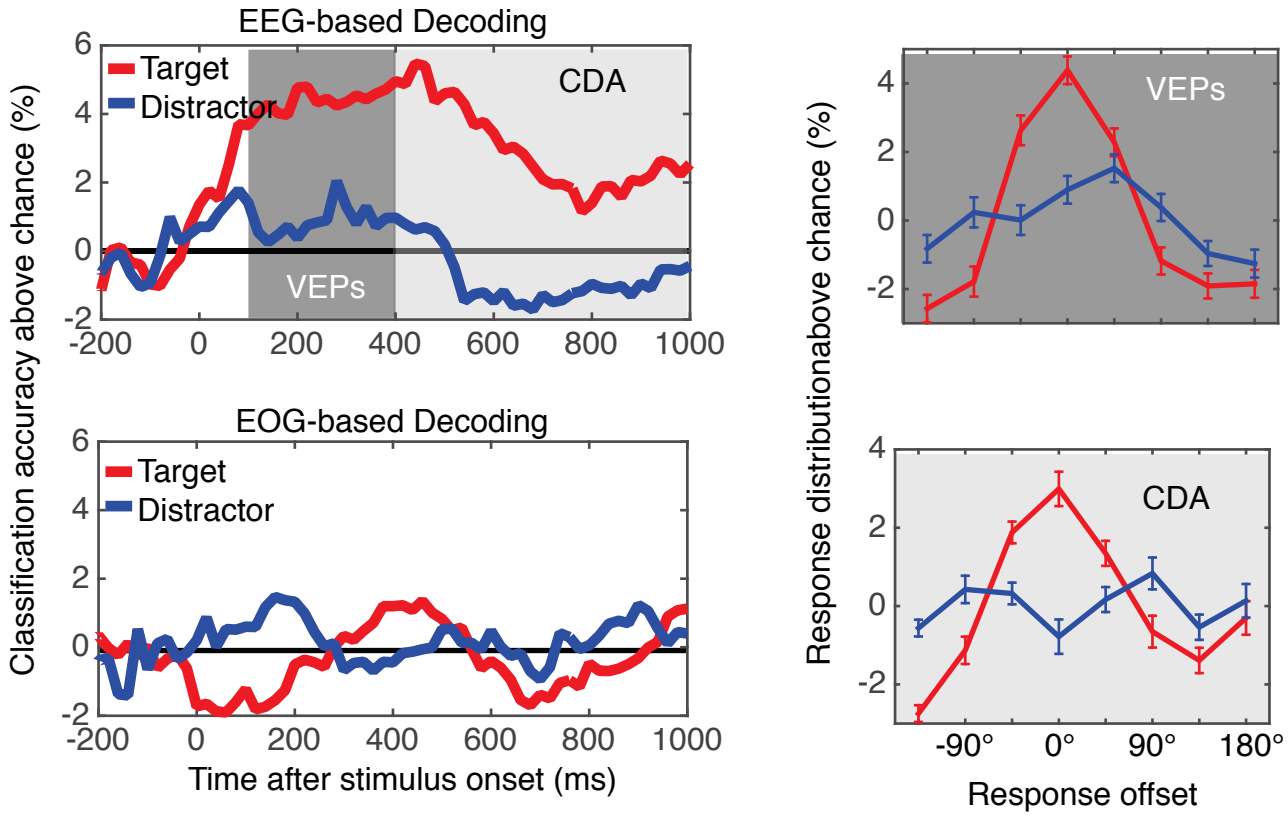


Figure 8. The ERP-based classification results from Experiment 3.
Top left and bottom left panels show the classification accuracy for the target (red) and distractor (blue) using the scalp distribution of the difference waves (i.e., contralateral-ipsilateral amplitudes) and EOG channels, respectively. Note that the laterality was defined with respect to the cued hemifield. The solid black line indicates the chance level of classification. The top right and bottom right panels show the distribution of response offsets produced by the VEPs-based decoder and the CDA-based decoder, respectively. The red lines show the result for target decoding, and the blue lines show that for distractor decoding. The error bars represent S.E.M.

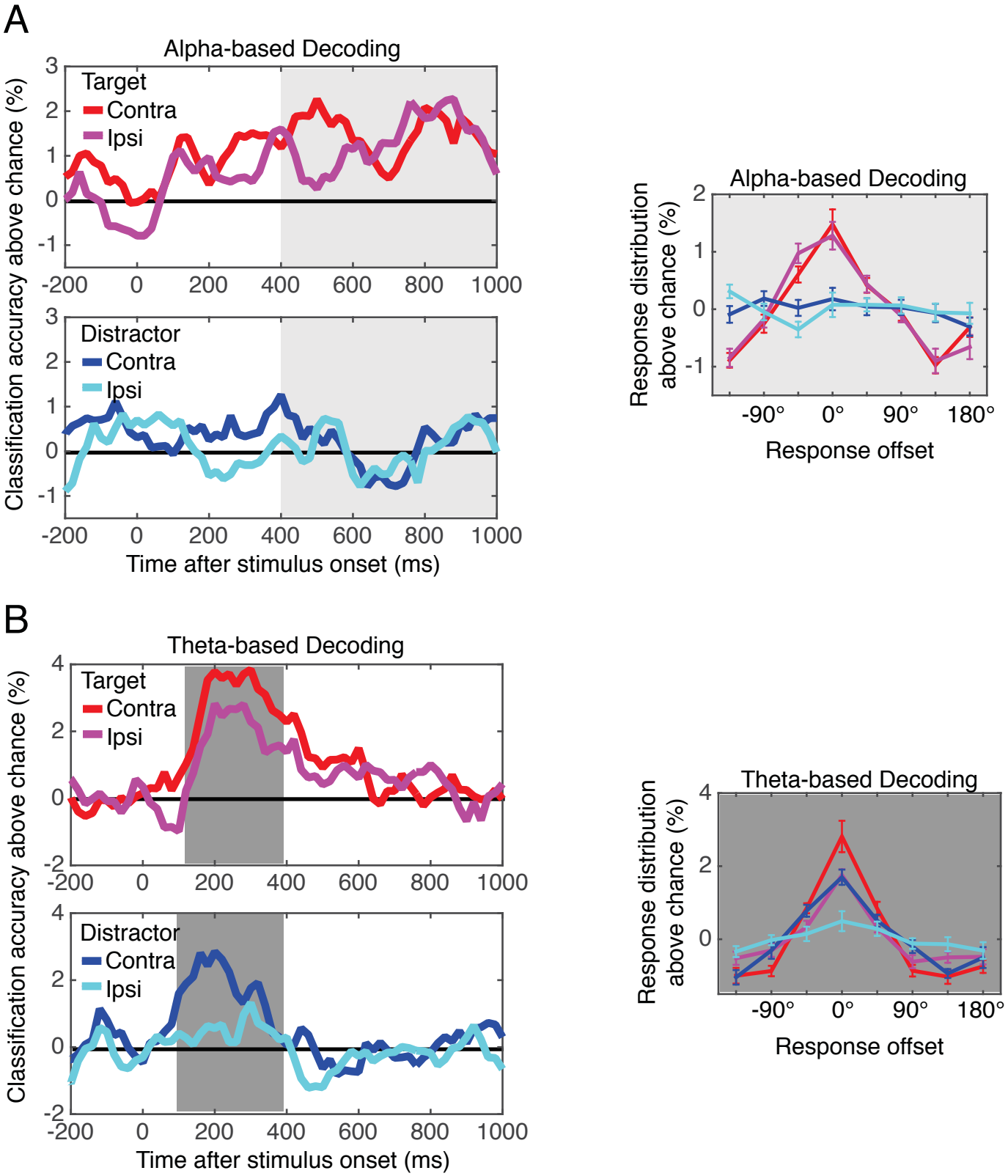


Figure 9. The oscillation-based classification results from Experiment 3.
Panel A) The results of the classification analyses based on the scalp distribution of alpha (8-12Hz) power. The top left figure shows the classification accuracy for target item using the scalp distribution of the contralateral (red) and ipsilateral (magenta) alpha power. The bottom left show the classification accuracy for distractor item based on contralateral (blue) and ipsilateral (cyan) alpha power distribution. Note that the laterality was defined with respect to the item of interest. The solid black line indicates the chance level of classification. The line graph on the left shows the distribution of response offsets produced by the alpha-power-based decoders. The red (contralateral) and magenta (ipsilateral) lines show the result for target decoding, and the blue (contralateral) and cyan (ipsilateral) lines show that for distractor decoding. The error bars represent S.E.M. Panel B) The results of the classification analyses based on the scalp distribution of theta (4-7Hz) power. The top left figure shows the classification accuracy for target item using the scalp distribution of the contralateral (red) and ipsilateral (magenta) theta power. The bottom left show the classification accuracy for distractor item based on contralateral (blue) and ipsilateral (cyan) theta power distribution. Note that the laterality was defined with respect to the item of interest. The solid black line indicates the chance level of classification. The line graph on the left shows the distribution of response offsets produced by the theta-power-based decoders. The red (contralateral) and magenta (ipsilateral) lines show the result for target decoding, and the blue (contralateral) and cyan (ipsilateral) lines show that for distractor decoding. The error bars represent S.E.M.

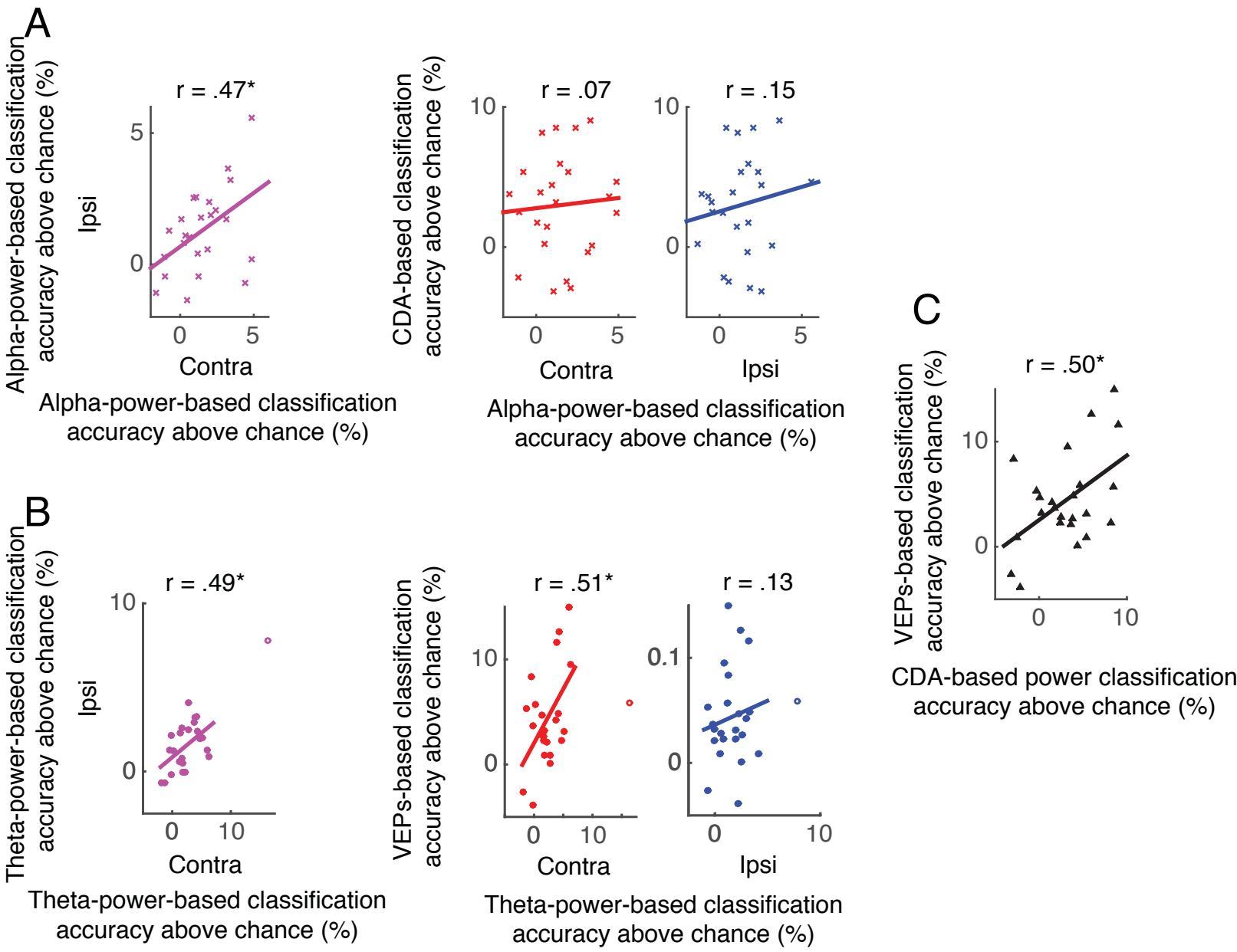


Figure 10. The results of correlational analyses from Experiment 3.
Panel A) Correlations between neural correlates of spatially global and lateralized VWM representations. The left scatter plot shows the correlation between decoding accuracies based on the scalp distributions of contralateral and ipsilateral alpha (8-12Hz) power. The right two scatter plots show the relationship between the decoding accuracies between the CDA-based and the contralateral alpha-power-based decoders (red) and between the CDA-based and the ipsilateral alpha-power-based decoders (blue). Panel B) Correlations between neural correlates of perceptual encoding. The left scatter plot shows the correlation between decoding accuracies based on the scalp distributions of contralateral and ipsilateral theta (4-7Hz) power. The right two scatter plots show the relationship between the decoding accuracies between the VEPs-based and the contralateral theta-power-based decoders (red) and between the VEPs-based and the ipsilateral theta-power-based decoders (blue). Panel C) The correlation between VEPs-based decoding performance and the CDA-based decoding performance. The asterisks represent the statistical significance of correlations (* = <.05).